Peer reviewed version

Link to published version (if available):
10.1109/TIA.2020.2975763

Link to publication record in Explore Bristol Research
PDF-document

University of Bristol - Explore Bristol Research
General rights

Additive Manufacturing of Shaped Profile Windings for Minimal AC Loss in Electrical Machines

N. Simpson and P. H. Mellor
Department of Electrical and Electronic Engineering
University of Bristol
Bristol, UK
nick.simpson@bristol.ac.uk

Abstract—**Concentrated wound, open slot, permanent magnet electrical machines are an attractive topology for automotive and aerospace applications as they exhibit compact end-windings, resulting in high power-density, facilitate fault tolerant operation through, physical, thermal, magnetic and electrical isolation of phase windings, and the open slot structure eases manufacture. However, a significant disadvantage of this topology is the interaction between the armature reaction field and winding conductors leading to elevated AC losses. A common mitigation technique is to reduce the height of the winding in the slot to minimise this interaction, however, the conductor cross-sectional area is consequently reduced which compromises low-speed performance. This paper investigates the use of additive manufacturing to produce shaped profile windings which exhibit minimal AC loss whilst maximising the utilisation of the slot area, thereby improving low-speed performance while maintaining high-speed performance.**

I. INTRODUCTION

Concentrated wound, open slot, Permanent Magnet (PM) electrical machines are an attractive topology for automotive and aerospace applications as they exhibit compact end-windings when compared to distributed wound machines, resulting in high power-density and efficiency, [1], [2], facilitate fault tolerant operation through, physical, thermal, magnetic and electrical isolation of phase windings, and the open slot structure eases manufacture, [1]–[3]. Typical operating requirements in these application areas include, [4], [5]:

- high torque- and power-density (minimal mass/volume)
- wide speed range operation
- wide constant power operation
- high efficiency across the operating range
- high torque at low speed (starting)
- high intermittent overload capability
- reliability and robustness
- low acoustic noise and vibration

With appropriate choice of pole-slot number and design, all these requirements can be addressed by an open-slot PM machine, however in high-frequency machines a significant disadvantage lies in the elevated AC winding losses due to a large exposure of the conductors to high magnetic fields around the slot opening, [6]. Where the hot-spot temperature of the windings ultimately dictates the electrical loading and hence torque capability of the machine as the winding current

must be limited to ensure that the temperature rating of the electrical insulation system is respected, [7].

A common AC loss mitigation technique is to reduce the height of the winding in the slot to minimise the field impinging on the conductors which results in improved high-frequency AC performance and lower peak-to-mean winding temperatures, however, the low-frequency DC performance is compromised since the slot area utilisation is poor, [8].

An alternative approach is to shape the profile of the conductors in the slot to minimise the interaction with the armature reaction field while maximising slot area utilisation. Shaped windings have been achieved using round wire wound on to forming bobbins, [9], by the use of pre-cut foil windings, [10], [11], through stacking a series of Printed Circuit Boards (PCBs) which are electrically connected in the end-winding or using solid busbar arrangements, [12]–[14]. More recently metal casting techniques have been explored, [15], [16], and the use of metal Additive Manufacturing (AM) methods have been demonstrated which offer unparalleled geometric freedom in conductor shape and layout, Fig. 1, and can allow additional features such as cooling channels and terminals to be built directly into the part, [17]–[21].

Fig. 1. Example of a shaped profile copper winding manufactured using Direct Metal Laser Sintering for a filter inductor application, [19].

In this paper, a method of determining an optimal shaped profile winding is presented which maximises slot area utilisation to achieve improved low-speed performance while maintaining low AC loss. The conductor shaping algorithm is demonstrated by the re-design of the windings of a 48V Integrated Starter Generator (ISG), [6] and aims to lay the foundation for design tools which can take advantage of the geometric freedom offered by present and future metal AM technologies.

II. Development of the Conductor Shaping Algorithm

The electrical machine topology under consideration, Section IV, features open stator slots and a PM rotor resulting in significant exposure of the concentrated windings to the slot leakage and rotor induced fields, Fig. 12. Hence, proximity to an external magnetic field is the dominant AC winding loss mechanism and is the focus of the conductor shaping algorithm, [22].

Consider an idealised rectangular conductor exposed to a uniform time varying external magnetic flux density, B, perpendicular to the surface, as illustrated in Fig. 2, where the conductor length, l, is assumed large compared to the width, w, and height, h, [23], [24]. The skin depth is assumed to be comparable to the conductor thickness such that the internal magnetic field is uniform, [25]. Faraday's law states that the magnetic flux, Φ, penetrating the loop $P_1 \rightarrow P_2 \rightarrow P_3 \rightarrow P_4$ will set up an electromotive force (EMF), e, according to, (1).
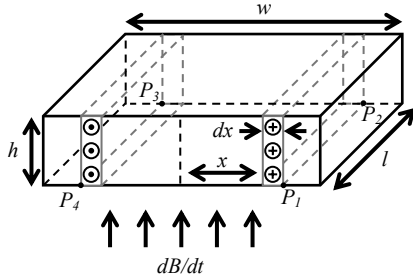

Fig. 2. Rectangular conductor exposed to a uniform time-varying external field, dB/dt, perpendicular to the surface.

$$e = \frac{d\Phi}{dt} = A\frac{dB}{dt} = 2xl\frac{dB}{dt} \quad (1)$$

$$R_{el} = \frac{2l}{\sigma dxh} \quad (2)$$

In turn the EMF induces an eddy current loop traversing the differential element, dx, with area, dxh, and length, l, into the page along $P_1 \rightarrow P_2$ and returning along $P_3 \rightarrow P_4$. The resistance of the eddy current loop, R_{el}, is given by (2) where, σ, is the electrical conductivity of the conductor. The power loss in the loop, P_{el}, is determined by (3) which yields the conductor power loss per unit length, P_{cond}, when integrated over the conductor surface, (4).

$$P_{el} = \frac{e^2}{R_{el}} = 2x^2 l\sigma h \left(\frac{dB}{dt}\right)^2 dx \quad (3)$$

$$P_{cond} = 2\int_0^{\frac{w}{2}} 2x^2\sigma h\left(\frac{dB}{dt}\right)^2 dx = \frac{w^3}{6}h\sigma\left(\frac{dB}{dt}\right)^2 \quad (4)$$

From inspection of (4), the per unit length power loss in the conductor, P_{cond}, is related to the cube of the exposed conductor width, w, and linearly to the exposed conductor height, h. Hence, the simplified model, Fig. 2, suggests that thin conductors ($w << h$) shaped to remain perpendicular to the external magnetic field will exhibit minimal loss. Therefore the conductor shaping algorithm must comprise:

- an electromagnetic slot model accounting for leakage and armature reaction fields capable of predicting AC conductor losses
- a method of determining magnetic flux direction information across the slot
- a method of distributing conductors and maintaining consistent conductor cross-sectional area
- a thermal model to account for the temperature dependence of electrical conductivity

A. Electromagnetic Slot Model

Although highly computationally efficient, analytical methods of estimating the armature reaction field, [26], [27], and AC losses within conductors, [8], [28], tend to require reformulation when the machine topology changes, assume linear magnetically permeable materials or are restricted to regular, repeated conductor shapes. Therefore a 2D Finite Element (FE) modelling approach is adopted which allows arbitrary shaped conductors to be easily represented and lends well to changes in machine topology.
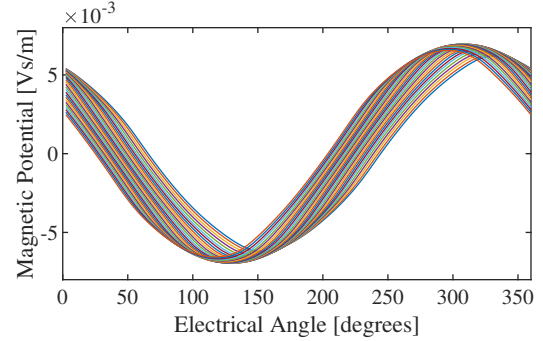
(a) Magnetic vector potential time-domain waveform observed at regular points along the slot opening.
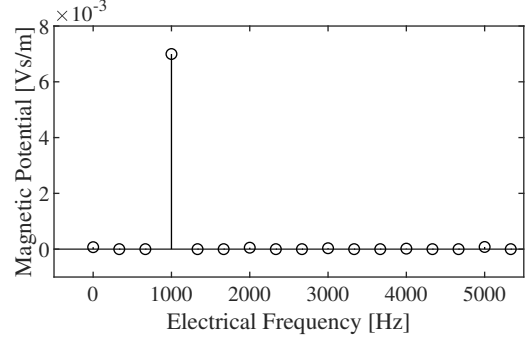
(b) Magnitude of frequency content of a magnetic vector potential time-domain waveform, Fig. 3a.

Fig. 3. Time and frequency domain magnetic vector potential at the slot opening, evaluated for a winding current of 75A and electrical frequency of, $f_{elec} = 1000$ Hz.

A time-stepping FE (TSFE) model would require a numerical field solution accounting for each shaped conductor to be calculated at each time-step as the rotor rotates within the stator, representing a significant computational overhead. As an alternative, a computationally efficient approximation based on a time-harmonic FE (THFE) model for the slot region can be used. Here, the armature reaction field is represented as a boundary condition by specifying the magnetic vector

potential, A, at regular points along the slot opening. The magnitude and phase of A at each point is obtained by extracting the time-domain A waveform, Fig. 3a, from corresponding points along the slot opening of a simplified (only lumped windings are modelled and symmetry is exploited) TSFE model, as illustrated in Fig. 3. Each waveform is decomposed into fundamental magnitude and phase components using a Fourier transform, Fig. 3b, and applied to the slot boundary of the THFE model. The TSFE model is evaluated for varying winding current and the resulting dataset interpolated to allow appropriate boundary conditions to be applied to the THFE model over the range of winding current and electrical frequency of interest without repeating the TSFE model analyses. The THFE model operates at a single frequency, f_{elec}, hence only the fundamental of the A waveform is accounted for, however, in this case the magnitude of the harmonics are negligible, Fig. 3.
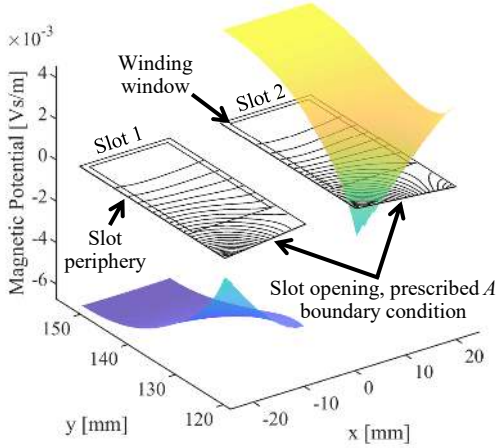

Fig. 4. Illustration of slot periphery and winding window with magnetic vector potential, representing the armature reaction field, plotted as a surface and as contours, winding current of 137.5 A, electrical frequency, $f_{elec} = 480$ Hz.

Fig. 4 illustrates the two stator slots occupied by a single concentrated winding along with the effective winding window area, accounting for slot liner and insulation. The magnetic vector potential obtained from the THFE slot model, accounting for slot leakage and rotor induced effects is plotted as a surface and as a series of contours for a winding current of 137.5A (60 Nm) and $f_{elec} = 480$ Hz (2400 RPM), Section IV. The contours shown are equipotentials of magnetic vector potential, A, the direction of which are parallel to the magnetic flux, Φ, [25], hence, the contours of A can be used to shape the profile of the conductors for minimum loss as illustrated in, Fig. 2 and (4).

The active-winding loss, P_{aw}, is estimated using the THFE model, showing close agreement with the TSFE model, as illustrated in Fig. 5. The end-winding loss, P_{ew}, is assumed to be DC only, (5), where I_{RMS}, N, $\bar{l}_{ew}$, $\bar{A}_c$ and σ_T are the RMS winding current, number of turns, the average end-winding length, average conductor cross-section and electrical conductivity at temperature, T, respectively.
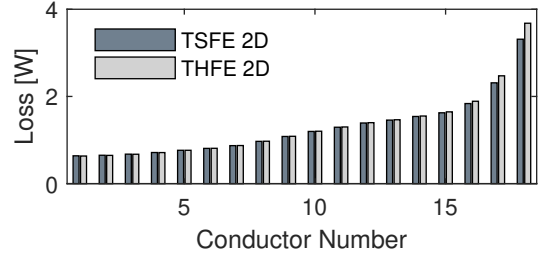
(a) AC conductor loss in slot 1.
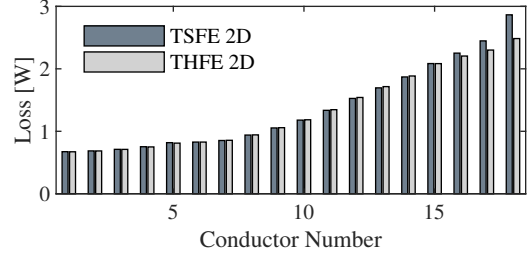
(b) AC conductor loss in slot 2.

Fig. 5. Conductor AC loss estimates from the TSFE and THFE models, $I = 75$ A and $f_{elec} = 1000$ Hz.

$$P_{ew} = I_{RMS}^2 R_{ew} = I_{RMS}^2 \frac{2N\bar{l}_{ew}}{\sigma_T \bar{A}_c} \tag{5}$$

B. Thermal Slot Model

The electrical conductivity and hence the induced losses of the conductor material are temperature dependent. The electrical conductivity, σ_T, at temperature, T, is given by (6) where $T_0 = 20$ °C, σ_{T_0}, and α are the reference temperature, electrical conductivity at the reference temperature and the temperature coefficient of resistance respectively.

$$\sigma_T = \frac{\sigma_{T_0}}{1 + \alpha (T - T_0)} \tag{6}$$

A 2D thermal conduction FE model, Fig. 6, is coupled with the electromagnetic THFE model, Section II-A, to iteratively calculate the conductor losses and temperature until a steady state is reached. As with the electromagnetic model, a 2D FE approach is favoured for the ease in which the stator and conductor geometry can be accurately represented. Temperature and loss calculations are performed at the conductor level to account for the variation in conductor loss and temperature resulting from the proximity to the electrical machine air-gap, [29]. The thermal model simulates a liquid cooled casing, Section IV, with a fixed temperature boundary condition on the stator outer diameter, $T_{coolant} = 60$ °C. The remaining boundaries are assumed to be adiabatic. The total winding loss, $P_{aw} + P_{ew}$, is assumed to be extracted through the active length of the winding in contact with the stator. The conductor insulation coating is neglected in the model to reduce computation time, rather, the material properties of the encapsulant and slot liner, Table I, are proportionally reduced from the manufacturer stated values to emulate the effect of contact conductance, conductor insulation and imperfect encapsulation, [7].
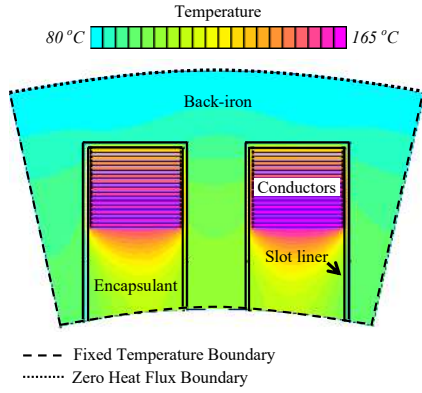
Fig. 6. Steady state thermal FE slot model.

TABLE I
MATERIAL THERMAL PROPERTIES

Material	Thermal Conductivity $[W/m.K]$	Adjusted Thermal Conductivity $[W/m.K]$
Conductor, CuCr1Zr	320	320†
Slot liner	0.2	0.1‡
Stator No20 SiFe	30	30
Encapsulant	0.85	0.4*

* Reduced to emulate conductor insulation and imperfect impregnation.
† Likely reduced by the AM process.
‡ Reduced to emulate contact conductance.

C. Conductor Shaping Algorithm

The conductor shaping algorithm seeks to distribute the conductors in such a way as to minimise the cross-sectional area exposed to the magnetic flux, Fig. 2 and (4). An overview of the algorithm is shown in Fig. 7. The THFE model is set up to simulate the desired operating point frequency, f_{elec}, and peak winding current, I. The conductors are initially distributed uniformly along the slot, assuming a single full-width column, as illustrated in Fig. 8a, which eases the manufacturing and electrical insulation process, [19], Section IV. The winding height, k_{wh}, is a design variable normalised to the slot dimensions, in this case $k_{wh} = 0.8$ or 80%. The electromagnetic slot model, Section II-A, is used to determine the initial magnetic vector potential across the slots, Fig. 4.

At the top of the slot, away from the air-gap, the flux traverses the slot in the x-direction almost parallel to the slot base, as shown in Fig. 4, hence the regular edge-wound conductors, Fig. 8a, are appropriate. Further down the slot, toward the air-gap, the flux ceases to be parallel to the slot base and conductors must be shaped, this point is referred to as the point of inflection, N_{inf}. In order to determine the shape of the conductors, the magnetic vector potential is sampled, A_{sn}, at the upper and lower boundary of each conductor to be shaped, coincident with a flux sampling line at $k_s = 0.95$ or 95%, normalised to the slot dimensions, as illustrated in Fig. 8b. The value of k_s is a design variable which strongly influences the overall winding shape. The contours of A are extracted based on each sample A_{sn} and used to construct a closed polygon, representing each conductor, shaped to run parallel to the flux lines. The change in winding shape alters
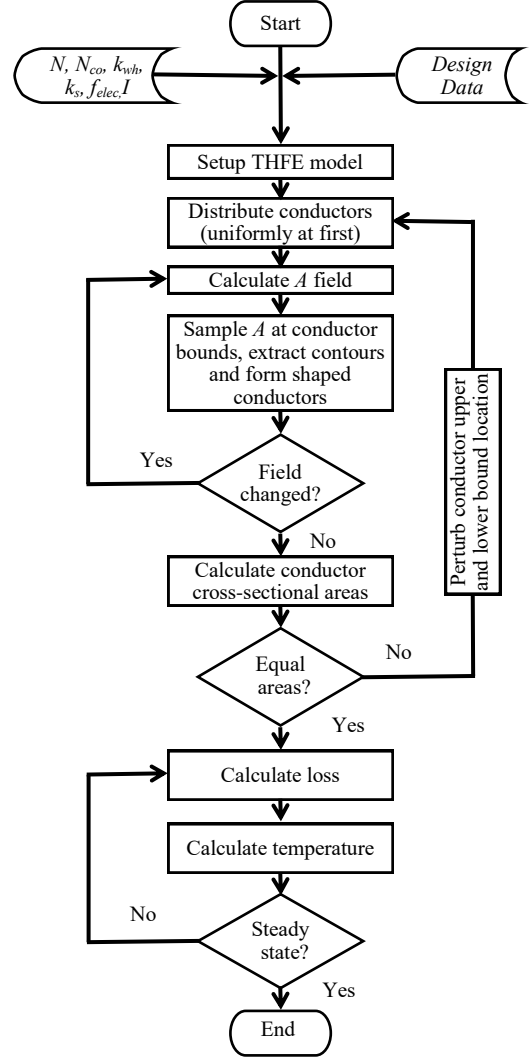

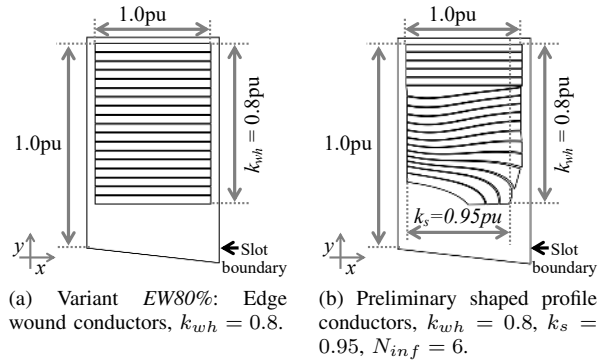Fig. 7. Overview of the conductor shaping algorithm.

(a) Variant *EW80%*: Edge wound conductors, $k_{wh} = 0.8$.

(b) Preliminary shaped profile conductors, $k_{wh} = 0.8$, $k_s = 0.95$, $N_{inf} = 6$.

Fig. 8. Edge wound and shaped profile winding examples, evaluated for an operating point of, $I = 75$ A$_{peak}$ and frequency, $f_{elec} = 480$ Hz (2400 RPM mechanical).

the magnetic field shape, hence, the process is repeated until a steady state is achieved. It is important to maintain an equal conductor cross-section throughout the winding so an optimisation routine, in this case Particle Swarm Optimisation (PSO), is used to perturb the y-coordinates of the magnetic vector potential sampling points, maintaining a monotonic or-

der, with the objective of achieving a consistent cross-sectional area, Fig. 8b. The performance of the resulting shaped profile windings is evaluated using the coupled electromagnetic and thermal models which are iteratively solved to yield the steady state loss and temperature profile.

III. EXPERIMENTAL MEASUREMENT OF ADDITIVELY MANUFACTURED MATERIAL SAMPLES

In order to provide accurate winding loss predictions, the electrical conductivity of the proposed AM material is required. The windings are intended to be manufactured using a copper-chromium-zirconium (CuCr1Zr) powder material through a Direct Metal Laser Sintering (DMLS) process. The DMLS process uses a high intensity energy source to selectively sinter powdered metal material in a succession of 2D scans, to incrementally build a 3D metal part, [30]. The sintered layer is re-coated with metal powder between each 2D scan. Once the part is complete, excess powder is removed and recycled before the part is separated from the metallic build platform using Electro Discharge Machining (EDM). The process parameters, such as layer thickness, applied power and build orientation along with post-processing steps, such as heat treating, dictate the surface finish, density and material properties of the part, [20].
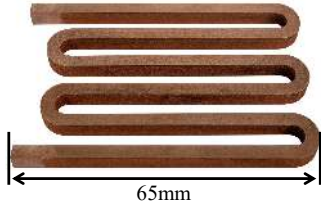

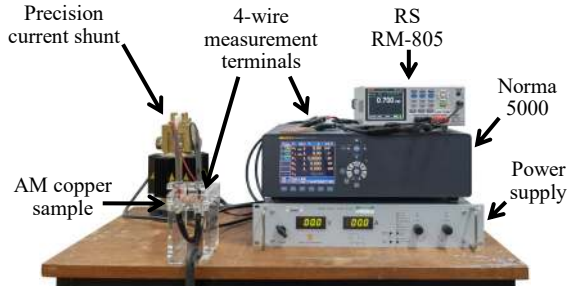Fig. 9. Sample of CuCr1Zr manufactured using DMLS, with a cross-section of 3×4 mm and 378 mm length.

Fig. 10. Experimental arrangement for the small signal and large signal measurement of electrical resistance.

$$\sigma = \frac{l}{R_{elec}A} \qquad (7)$$

TABLE II
AM COPPER SAMPLE RESISTANCE MEASUREMENTS

	Electrical Resistance, R_{elec}, [mΩ]		
Sample Number	RS RM-805	Norma 5000	% IACS [%]
1	0.71	0.70	77.7
2	0.69	0.69	78.3
3	0.70	0.71	76.8
4	0.71	0.70	77.6

Standard electrical wire grade copper (C11000) has a typical electrical conductivity of $\sigma = 58$ MS/m representing 100 % International Annealed Copper Standard (IACS) whereas CuCr1Zr (C18150) exhibits 76-90% IACS or $\sigma = 44 - 52$ MS/m, [31]. However, the electrical conductivity of built parts must be experimentally measured to account for the process parameters and any post-processing steps. Batches of DMLS material samples were manufactured using differing sets of process parameters and post-processing steps, Fig. 9, with geometry in accordance with ASTM B193-16, [32]. The electrical resistance of the material samples is measured using a small signal (1 A) RS RM-805 4-wire Ohm meter and a large signal (40 A) Norma 5000 with precision current shunt and 4-wire terminal arrangement as shown in Fig. 10. All measurements were performed at room temperature ($T_0 = 21$ ºC) with short measurement intervals to avoid self-heating of the samples. The electrical conductivity is calculated from the measured electrical resistance, R_{elec}, sample cross-sectional area, A, and mean path length, l, (7). Of the material sample batches measured, the highest electrical conductivity is 77.6% IACS averaged over the 4 material samples in the batch, with a standard deviation of 0.6 %, Table II. A conservative $\sigma = 75\%$ IACS is assumed throughout the remaining analysis.

IV. ELECTRICAL MACHINE CASE STUDY

The conductor shaping algorithm is demonstrated through the re-design of the $N = 18$ turn windings of a brushless Permanent Magnet (PM) automotive ISG, Fig. 12, [6]. The ISG is a variant of the 10 pole, $p = 10$, 12 slot, $q = 12$, topology with a single-layer three-phase concentrated winding and a quasi-Halbach PM array on the rotor. The ISG must conform to a strict space envelope within the drivetrain, as such the stator diameter to active length ratio is 9.4 with an active length of 35mm. The torque-speed characteristic of the baseline machine is illustrated in Fig. 11, additional design data is given in Table III.
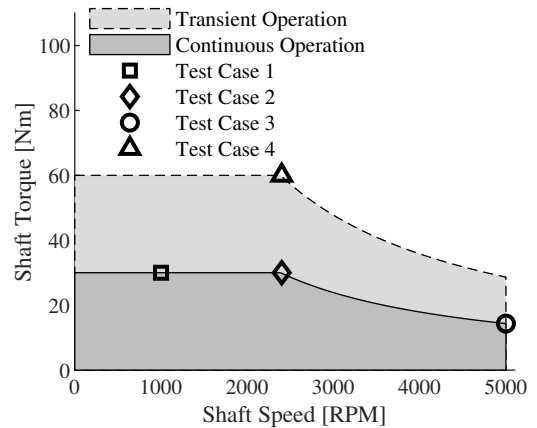

Fig. 11. Continuous and transient torque-speed curves of the ISG, [6].

TABLE III
ISG SPECIFICATION

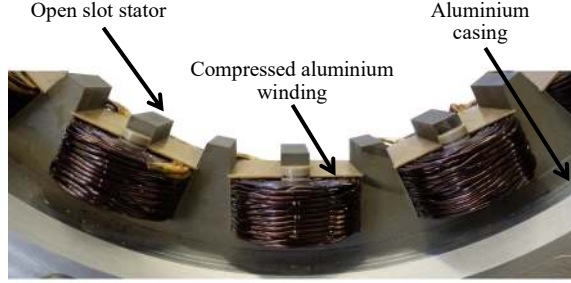| Parameter	Value
Package volumetric envelope	3.6 L
Maximum rated rotational speed	5000 RPM
Continuous power/torque rating	7.5 kW / 30 Nm
Transient power/torque rating	15 kW / 60 Nm
Nominal voltage	48 V
Torque constant	0.4 Nm/A
Active length	35 mm

Fig. 12. Image of a three-phase span of the ISG, rotor not present.

V. SHAPED PROFILE WINDING DESIGN

Three variants of the $N = 18$ turn ISG windings are designed and compared in order to demonstrate the effect of conductor location and shape on performance. The first variant, *EW80%*, is edge-wound with a winding height of $k_{wh} = 0.8$, Fig. 8a, the second variant, *EW50%*, is edge-wound with a winding height of $k_{wh} = 0.5$, Fig. 13a, and the final variant, *Shaped*, is a shaped profile winding, Section II, with a winding height of $k_{wh} = 0.8$, flux sampling point of $k_s = 0.95$ and inflection point of $N_{inf} = 6$, Fig. 13b. The windings are designed for an operating point of, $I = 137.5$ A$_{peak}$, and frequency, $f_{elec} = 480$ Hz (2400 RPM mechanical), Fig. 11.

(a) Variant *EW50%*: Edge wound conductors, $k_{wh} = 0.8$.

(b) Variant *Shaped*: Shaped profile conductors, $k_{wh} = 0.8$, $k_s = 0.95$, $N_{inf} = 6$.
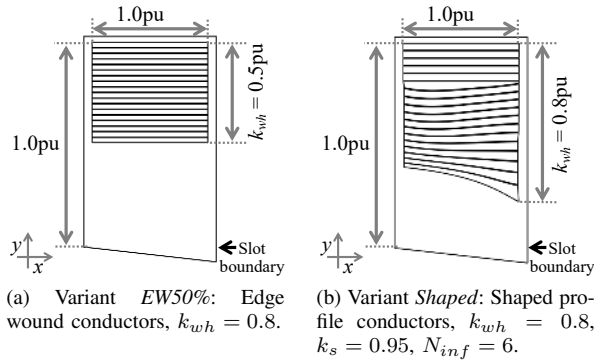
Fig. 13. Edge wound and shaped profile winding variants, evaluated for an operating point of, $I = 137.5$ A$_{peak}$ and frequency, $f_{elec} = 480$ Hz (2400 RPM mechanical).

The variation of magnetic vector potential across each of the slots, Fig. 4, leads to an asymmetric conductor profile, Fig. 14. Hence, the winding loss is dependent upon the rotational direction of the rotor shaft, however, many applications such as generators, fans and traction drives primarily require rotation in a single direction. The asymmetric conductor profiles must be merged in the end winding to form a complete concentrated

winding as illustrated in Fig. 15 where the end-windings are semi-square rather than semi-circular, [19], to minimise the end-winding length, reduce losses and improve power-density.
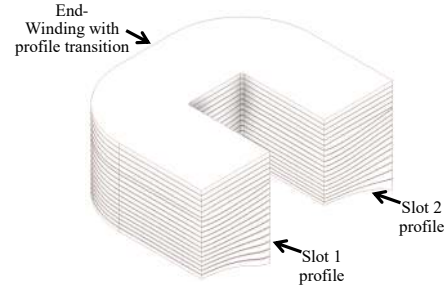

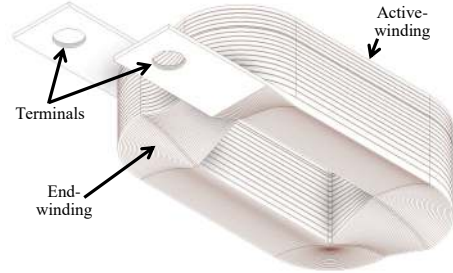Fig. 14. Active length profiles of the *shaped* winding variant, Fig. 13b.

Fig. 15. Illustration of the complete shaped profile winding design.

VI. RESULTS AND DISCUSSION

In order to validate the assumption of DC loss in the end-winding, Section II-A, 3D time-stepping FE is used to predict the total loss of the shaped profile winding at 20 ºC for the four test cases given in Table IV and Fig. 11. The 3D TSFE model and the 2D THFE model with DC end winding loss show close agreement with a maximum deviation of < 10%, Table V.

TABLE IV
MODEL VALIDATION TEST CASES

Test Case	Shaft Speed [RPM]	Shaft Torque [Nm]	Electrical Frequency [Hz]	Peak Winding Current [A]
1	1000	30	200	75.0
2	2400	30	480	75.0
3	5000	14	1000	35.0
4	2400	60	480	137.5

Fig. 16 shows the predicted winding loss of the three winding variants over the operating frequency range evaluated at $I = 137.5$ A$_{peak}$ corresponding to 60 Nm shaft torque. Winding variant *EW80%* exhibits the lowest loss at DC due to the high slot area utilisation, however, the proximity to the high fields in the slot opening region induces large AC losses which are a strong function of frequency leading to high operating temperatures, Fig. 17, and a worst case variation in conductor temperature of 82 ºC. Winding variant *EW50%* resides lower in the slot to minimise the interaction with the armature reaction field, Fig. 13a, resulting in an AC loss profile which is a weak function of frequency, however, the poor slot

TABLE V
MODEL VALIDATION RESULTS

Test Case	Model Type	Active Length Loss [W]	End-Winding[†] Loss [W]	Total Winding Loss [W]
1	TSFE 3D	N/A	N/A	12.9
	TSFE 2D	7.9	6.5	14.4
	THFE 2D	7.8	6.5	14.3
2	TSFE 3D	N/A	N/A	17.1
	TSFE 2D	11.7	6.5	18.2
	THFE 2D	11.5	6.5	18.0
3	TSFE 3D	N/A	N/A	18.9
	TSFE 2D	19.1	1.4	20.5
	THFE 2D	18.5	1.4	19.9
4	TSFE 3D	N/A	N/A	46.3
	TSFE 2D	25.4	22.0	47.4
	THFE 2D	24.9	22.0	46.9

[†] Assumed to be DC loss, evaluated at the RMS winding current.

area utilisation compromises the DC performance leading to relatively high winding loss across the operating frequency range. Winding variant *Shaped* exhibits a 35% greater slot area utilisation than *EW50%* giving a corresponding improvement in DC performance. The shaped conductors conform to the magnetic flux lines, minimising AC loss, however the AC loss profile is a stronger function of frequency than *EW50%* as shown by the difference in gradient. Nonetheless, the *Shaped* winding exhibits lower loss and operating temperatures across the frequency range.
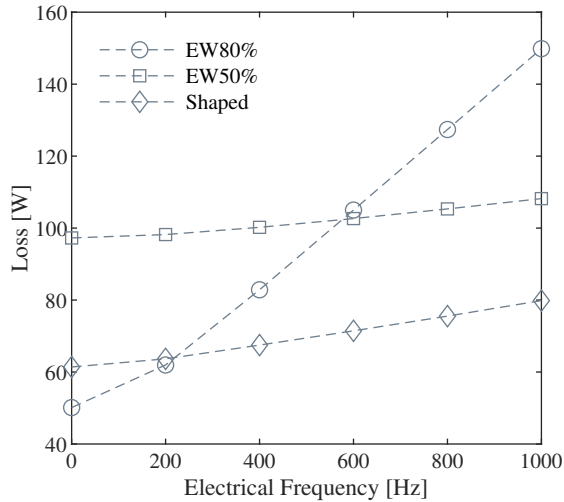

Fig. 16. Winding loss prediction of the three winding variants for $I = 137.5$ A_{peak}.

Fig. 18 shows the steady state current carrying capacity and torque production capability of the winding variants over the operating frequency range assuming a steady state average winding temperature of 180 °C commensurate with a class H electrical insulation rating. As expected, variant *EW80%* exhibits the highest starting torque owing to the lowest DC resistance, however, the performance drops rapidly as frequency increases. It should be noted that this winding is capable of meeting the baseline machine specification, Fig. 11. Winding variant *EW50%* is capable of continuously operating with an output torque of approximately 50 Nm, exceeding the specification. Transient operation of 60 Nm is likely possible
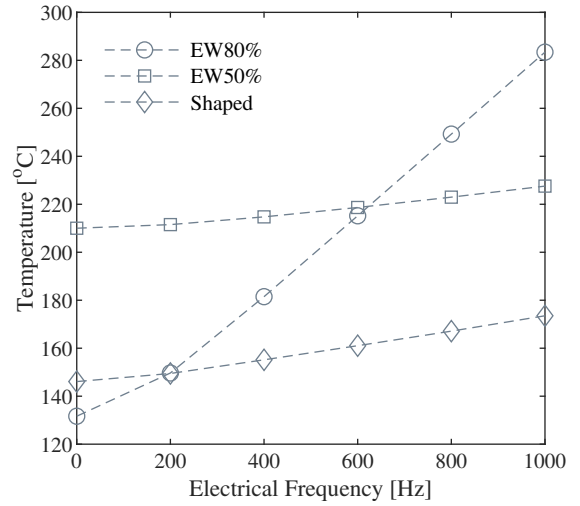

Fig. 17. Steady state average winding temperature prediction of the three winding variants for $I = 137.5$ A_{peak}.
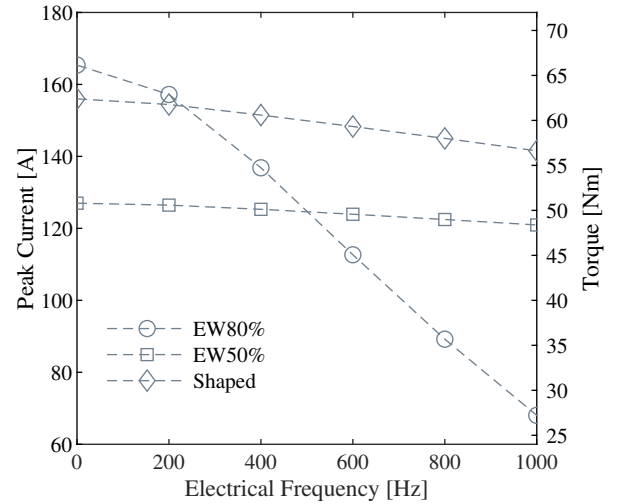

Fig. 18. Predicted continuous operating envelope assuming a 180 ° C average absolute winding temperature.

for very short durations only since the thermal capacity of the physically smaller winding is low and the DC resistance is comparatively high. The *Shaped* winding offers a favourable compromise between DC and AC performance enabling a continuous average torque output of 60 Nm over the frequency range representing a 20% improvement over winding variant *EW50%* in spite of the AC losses being a stronger function of frequency. In addition, the transient performance of the *Shaped* winding is improved over the *EW50%* variant owing to the larger volume and thermal capacity.

VII. CONCLUSION

This paper presents an algorithm intended to shape the profile of winding conductors to minimise AC loss whilst increasing slot area utilisation, thereby reducing losses and increasing specific output across the operating frequency range. The resulting winding shape is highly dependent upon the design variables described in Section II-C and will be explored

in further work. In this case study, a 20% improvement in continuous output capability is observed. Further, significantly greater performance improvements were indicated for transient operation over the operational torque-speed envelope. The algorithm is applicable, but not limited to, open slot electrical machine topologies. Present research is focused on solid conductor windings with relatively few turns to take advantage of good thermal performance (high conductor to insulation ratio) and ease manufacture. Accurate DMLS material data was obtained experimentally with the electromagnetic and thermal winding performance results verified using 2D and 3D FE. Further work includes the manufacture and experimental test of the *Shaped* winding within the prototype electrical machine, Fig. 12. Additive manufacturing of shaped profile windings has been shown to be a promising technology in the improvement of specific output of electrical machines and this paper lays the foundation for design tools which can take advantage of the unparalleled geometric freedom offered by present and future metal AM technologies.

REFERENCES

[1] A. M. EL-Refaie, "Fractional-slot concentrated-windings synchronous permanent magnet machines: Opportunities and challenges," *IEEE Transactions on Industrial Electronics*, vol. 57, no. 1, pp. 107–121, Jan 2010.
[2] F. Magnussen and C. Sadarangani, "Winding factors and joule losses of permanent magnet machines with concentrated windings," in *Electric Machines and Drives Conference, 2003. IEMDC'03. IEEE International*, vol. 1, June 2003, pp. 333–339 vol.1.
[3] A. G. Sarigiannidis, M. E. Beniakar, P. E. Kakosimos, A. G. Kladas, L. Papini, and C. Gerada, "Fault tolerant design of fractional slot winding permanent magnet aerospace actuator," *IEEE Transactions on Transportation Electrification*, vol. 2, no. 3, pp. 380–390, Sept 2016.
[4] Z. Q. Zhu and C. C. Chan, "Electrical machine topologies and technologies for electric, hybrid, and fuel cell vehicles," in *2008 IEEE Vehicle Power and Propulsion Conference*, Sept 2008, pp. 1–6.
[5] K. T. Chau, C. C. Chan, and C. Liu, "Overview of permanent-magnet brushless drives for electric and hybrid electric vehicles," *IEEE Transactions on Industrial Electronics*, vol. 55, no. 6, pp. 2246–2257, June 2008.
[6] R. Wrobel, N. Simpson, P. H. Mellor, J. Goss, and D. A. Staton, "Design of a brushless pm starter generator for low-cost manufacture and a high-aspect-ratio mechanical space envelope," *IEEE Transactions on Industry Applications*, vol. 53, no. 2, pp. 1038–1048, March 2017.
[7] N. Simpson, R. Wrobel, and P. H. Mellor, "Estimation of equivalent thermal parameters of impregnated electrical windings," *IEEE Transactions on Industry Applications*, vol. 49, no. 6, pp. 2505–2515, Nov 2013.
[8] P. Mellor, R. Wrobel, and N. Simpson, "Ac losses in high frequency electrical machine windings formed from large section conductors," in *2014 IEEE Energy Conversion Congress and Exposition (ECCE)*, Sept 2014, pp. 5563–5570.
[9] C. R. Sullivan, J. D. McCurdy, and R. A. Jensen, "Analysis of minimum cost in shape-optimized litz-wire inductor windings," in *2001 IEEE 32nd Annual Power Electronics Specialists Conference (IEEE Cat. No.01CH37230)*, vol. 3, 2001, pp. 1473–1478 vol. 3.
[10] J. D. Pollock and C. R. Sullivan, "Loss models for shaped foil windings on low-permeability cores," in *2008 IEEE Power Electronics Specialists Conference*, June 2008, pp. 3122–3128.
[11] ——, "Gapped-inductor foil windings with low ac and dc resistance," in *Conference Record of the 2004 IEEE Industry Applications Conference, 2004. 39th IAS Annual Meeting.*, vol. 1, Oct 2004, p. 557.
[12] D. C. Pentz and I. W. Hofsajer, "A performance evaluation of shaped planar inductor windings in gapped core applications utilizing turns with constant dc-resistance," in *2007 IEEE Power Engineering Society Conference and Exposition in Africa - PowerAfrica*, July 2007, pp. 1–6.
[13] T. Nomura, C. M. Wang, K. Seto, and S. W. Yoon, "Planar inductor with quasi-distributed gap core and busbar based planar windings," in *2013 IEEE Energy Conversion Congress and Exposition*, Sept 2013, pp. 3706–3710.
[14] K. D. T. Ngo, R. P. Alley, and A. J. Yerman, "Fabrication method for a winding assembly with a large number of planar layers," *IEEE Transactions on Power Electronics*, vol. 8, no. 1, pp. 55–61, Jan 1993.
[15] M. Gröninger, F. Horch, A. Kock, M. Jakob, and B. Ponick, "Cast coils for electrical machines and their application in automotive and industrial drive systems," in *2014 4th International Electric Drives Production Conference (EDPC)*, Sept 2014, pp. 1–7.
[16] M. Gröninger, F. Horch, A. Kock, H. Pleteit, B. Ponick, D. Schmidt, and F. J. Wöstmann, "Casting production of coils for electrical machines," in *2011 1st International Electric Drives Production Conference*, Sept 2011, pp. 159–161.
[17] C. Wohlers, P. Juris, S. Kabelac, and B. Ponick, "Design and direct liquid cooling of tooth-coil windings," *Electrical Engineering*, Jul 2018. [Online]. Available: https://doi.org/10.1007/s00202-018-0704-x
[18] J. P. Rigla, A. Sarwar, A. Nacev, M. G. Urdaneta, E. Anashkin, P. Stepanov, I. N. Weinberg, J. M. Benlloch, A. McMillan, R. Hilaman, and S. T. Fricke, "Design and additive manufacturing of mri gradient coils," in *2014 IEEE Nuclear Science Symposium and Medical Imaging Conference (NSS/MIC)*, Nov 2014, pp. 1–4.
[19] N. Simpson and P. H. Mellor, "Additive manufacturing of shaped profile windings for minimal ac loss in gapped inductors," in *2017 IEEE International Electric Machines and Drives Conference (IEMDC)*, May 2017, pp. 1–7.
[20] C. Silbernagel, I. Ashcroft, P. Dickens, and M. Galea, "Electrical resistivity of additively manufactured alsi10mg for use in electric motors," *Additive Manufacturing*, vol. 21, pp. 395 – 403, 2018. [Online]. Available: http://www.sciencedirect.com/science/article/pii/S2214860418300769
[21] R. Ranjan and J. Tangudu, "Thermal design of high power-density additively-manufactured induction motors," in *2014 IEEE Energy Conversion Congress and Exposition (ECCE)*, Sept 2014, pp. 1325–1331.
[22] M. Popescu and D. G. Dorrell, "Skin effect and proximity losses in high speed brushless permanent magnet motors," in *2013 IEEE Energy Conversion Congress and Exposition*, Sept 2013, pp. 3520–3527.
[23] C. R. Sullivan, "Computationally efficient winding loss calculation with multiple windings, arbitrary waveforms, and two-dimensional or three-dimensional field geometry," *IEEE Transactions on Power Electronics*, vol. 16, no. 1, pp. 142–150, Jan 2001.
[24] D. C. Pentz and I. W. Hofsajer, "Novel technique for shaped planar inductor winding optimization in gapped core applications," in *2007 IEEE Power Engineering Society Conference and Exposition in Africa - PowerAfrica*, July 2007, pp. 1–6.
[25] P. Hammond, *Applied electromagnetism*. Elsevier, 2013.
[26] C. Ma, Q. Li, H. Lu, Y. Liu, and H. Gao, "Analytical model for armature reaction of outer rotor brushless permanent magnet dc motor," *IET Electric Power Applications*, vol. 12, no. 5, pp. 651–657, 2018.
[27] A. Dalal and P. Kumar, "Analytical model for permanent magnet motor with slotting effect, armature reaction, and ferromagnetic material property," *IEEE Transactions on Magnetics*, vol. 51, no. 12, pp. 1–10, Dec 2015.
[28] Y. Amara, P. Reghem, and G. Barakat, "Analytical prediction of eddy-current loss in armature windings of permanent magnet brushless ac machines," *IEEE Transactions on Magnetics*, vol. 46, no. 8, pp. 3481–3484, Aug 2010.
[29] R. Wrobel and N. Simpson, "Winding loss separation in thermal analysis of electromagnetic devices," in *2016 XXII International Conference on Electrical Machines (ICEM)*, Sept 2016, pp. 2133–2139.
[30] W. E. Frazier, "Metal additive manufacturing: A review," *Journal of Materials Engineering and Performance*, vol. 23, no. 6, pp. 1917–1928, Jun 2014. [Online]. Available: https://doi.org/10.1007/s11665-014-0958-z
[31] M. Jovanović and V. Rajković, "High electrical conductivity cu-based alloys, part i," *Metalurgija*, vol. 15, no. 2, pp. 125–133, 2009.
[32] A. International, "Astm b193-16 standard test method for resistivity of electrical conductor materials," *ASTM*, 2013. [Online]. Available: www.astm.org